$$P_1 = \begin{bmatrix} \cos(\alpha) & -\sin(\alpha) \\ \sin(\alpha) & \cos(\alpha) \end{bmatrix} \begin{bmatrix} \frac{1}{\sqrt{1+\varepsilon^2}} \\ i\frac{\varepsilon}{\sqrt{1+\varepsilon^2}} \end{bmatrix}, \tag{4}$$

$$P_2 = \begin{bmatrix} \cos\left(\alpha+\frac{\pi}{2}\right) & -\sin\left(\alpha+\frac{\pi}{2}\right) \\ \sin\left(\alpha+\frac{\pi}{2}\right) & \cos\left(\alpha+\frac{\pi}{2}\right) \end{bmatrix} \begin{bmatrix} \frac{1}{\sqrt{1+\varepsilon^2}} \\ i\frac{-\varepsilon}{\sqrt{1+\varepsilon^2}} \end{bmatrix}. \tag{5}$$

The major challenge for this model of the propagation is the limited information about the exact dispersion data and about the optical activity parameters of quartz [17–19]. We fitted the available data for quartz [20] in the wavelength range from 404 to 1160 nm with the Sellmeyer equation (Eq. (6) and Table 1.), which we used for the first propagation step in combination with the dispersion formulas given by Dodge et al. [21] for MgF_2. The necessary data for the second propagation step through the retardation plate used by Eckle et al. [7] has been kindly provided by its manufacturer Bernhard Halle Nachfolger GmbH and are shown in Fig. 2.

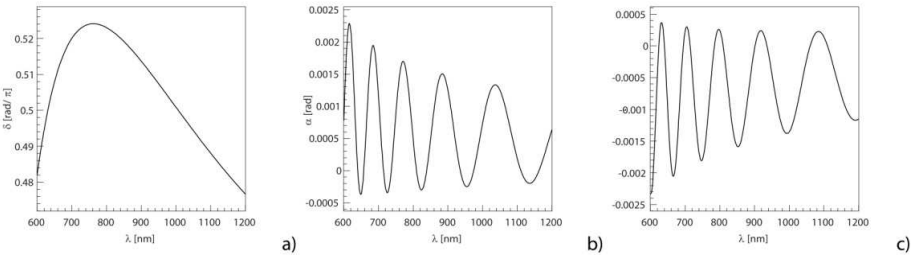

Fig. 2. Parameters of the λ/4 waveplate: a) Phaseshift δ, b) rotation angle α of the eigenmodes, c) ellipticity parameter ε.

$$n_i^2 - 1 = \sum_{j=1}^{6} \frac{A_j \lambda^2}{\lambda^2 - \lambda_j^2}. \tag{6}$$

Table 1. Parameters in Eq. (6)

	$\mathbf{n_o}$	$\mathbf{n_e}$
$\mathbf{A_1}$	0.34418	0.34057
$\mathbf{A_2}$	0.33846	0.33721
$\mathbf{A_3}$	0.33487	0.3486
$\mathbf{A_4}$	0.33949	0.35784
$\mathbf{A_5}$	6.64134	6.59729
$\mathbf{A_6}$	6.8756	6.66729
$\boldsymbol{\lambda_1}$	0.00514	0.00515
$\boldsymbol{\lambda_2}$	0.00531	0.00532
$\boldsymbol{\lambda_3}$	0.054	0.00533
$\boldsymbol{\lambda_4}$	0.01558	0.015792
$\boldsymbol{\lambda_5}$	1166.36478	1091.96331
$\boldsymbol{\lambda_6}$	1192.17287	1106.31822

#129004 - $15.00 USD Received 25 May 2010; revised 23 Jul 2010; accepted 23 Jul 2010; published 2 Aug 2010
(C) 2010 OSA

The spectrum of the pulse used by Eckle et al. [7] extends the region of the supplied data to shorter wavelength by 50 nm. This region contains 2.5% of the pulse energy, so the error introduced by cubic spline extrapolation of the retardation plate specifications into this region will not lead to a significant amount of error, especially since the parameter with strongest impact on the electric field δ shows a smooth behavior and can safely be extrapolated. The resulting pulse has a FWHM of 5.9 fs and exhibits a time dependent ellipticity as shown in Fig. 3. The ellipticity becomes visible as a wave-like modulation on a smooth pulse envelope. The position in time of the maxima in the modulation changes as a function of the CEO phase of the pulse. This results from the combination of the rotation of the direction of the electric field of the entire pulse due to the change of the CEO phase, and the fact that the axes of the polarization are fixed in laboratory frame by the position of the retardation plate. The time-dependent ellipticity can be expressed by the quotient of the axes of the polarization ellipse by the use of the Stokes parameter [22]. The ellipticity lies between 5 and 10 percent in the region of ± 5 fs around the pulse center as shown in Fig. 3.

3. Final momentum distribution using ADK rate and Newtonian motion

As shown by Eckle et al. [7], ellipticity changes the CEO-dependent behavior of the electron momentum distribution. The maximum flips from one lobe of the distribution to the other, see Fig. 4, instead of the smooth rotation expected for perfect circular polarization. The rotation expected for an ideal circular pulse is seen only after the momentum distribution is divided by a CEO phase-averaged distribution (Fig. 4). In this section, we introduce a simple method for calculating electron momentum distributions that reproduces the effects measured by Eckle et al. [7]. We combine the ADK tunnel theory with classical 2D particle propagation in the calculated field from section one to obtain the momentum distributions. The classical propagation is done in velocity space since only the particle momentum can be obtained from the experimental data, which also reduces the computational time. To match the quantum mechanical momentum distribution we use the predictions of the extended ADK theory [23]. If not stated otherwise, atomic units are used throughout the paper. Within this approach, the ionization rate w_s for circular polarized, stochastic light [23] is given by Eq. (7):

$$w_s \sim \exp\left(-\frac{3^{\frac{1}{3}}}{E^{\frac{2}{3}}}\left[2\varepsilon_i + p_\perp^2 + (p_\parallel - \frac{E^*}{\omega})^2 \right] \right) \text{ with } E^* = E^{\frac{2}{3}}(2\varepsilon_i)^{\frac{1}{2}} 3^{-\frac{1}{3}}. \tag{7}$$

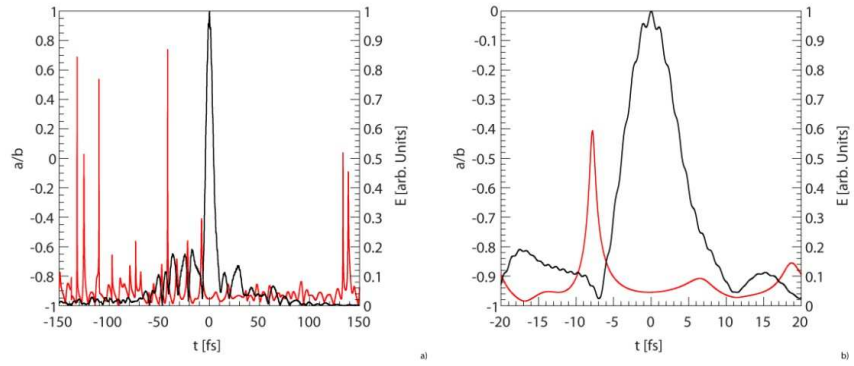

Fig. 3. a) Pulse shape (black curve, right scale) and ellipticity (red curve, left scale). b) zoom into central region of a). We used a typical pulse shape of the electric field of the laser pulses from experimental data. The time dependent ellipticity is expressed as the ratio of the two major axis of polarization; the sign represents the helicity.

#129004 - $15.00 USD Received 25 May 2010; revised 23 Jul 2010; accepted 23 Jul 2010; published 2 Aug 2010
(C) 2010 OSA

where E is the electric field strength, ε_i the ionization potential and ω the angular frequency of the laser light. Delone and Krainov used $p_\parallel$ as the final momentum of the electron in the polarization plane and $p_\perp$ as the final electron momentum perpendicular to it. This extension provides a momentum distribution along and perpendicular to the polarization directions for non-monochromatic circularly polarized light. Since we ignore the Coulomb potential and the spatial dependence of the electric field in our semiclassical model, the initial momentum distribution, centered at momentum 0 is transferred into the final momentum distribution by an offset equal to the momentum gained by the electron on its classical trajectory. To adapt the momentum distribution of Eq. (7) for an instantaneous ionization, we change the interpretation of $p_\perp$ to the momentum perpendicular to the electric field vector at the instant of ionization. In tunneling theories the electron has zero velocity after tunneling through the potential barrier. We therefore shift the distribution of $p_\parallel$ by E^*/ω to zero. We use this adapted momentum distribution to provide initial conditions for the classical trajectories starting at t_i with an electric field strength $E = E(t_i)$. Momentum frequency distributions are created for all distributions numerically using the acceptance–rejection method. Substituting the shifted $p_\parallel$ in Eq. (7), this equation can be written as a product of three exponential functions, each of them depending either on the ionization potential, the shifted $p_\parallel$ or $p_\perp$, showing the statistical independence of this quantities. Motivated by this independence we used Eq. (7) for the momentum distribution and the ionization rate was calculated by the ADK-formula for circularly polarized light [11].

The propagation of the electron after it has tunneled through the potential barrier is modeled by solving numerically the equation of motion in the electric field of the laser pulse by the Runge-Kutta 4th order method [24] in velocity space. We have used equally spaced instants of ionization in the time interval ± 5 fs in time steps of 0.01 fs around the center of the laser pulse. The ionization probability outside this time interval can be neglected for a 5.9 fs laser pulse with the intensity of 3.92 10^{14} W/cm^2. The electron is then propagated in the electric field with no spatial dependency up to 200 fs after the pulse center. To match the experimental ion data, the temperature of the gas target of 2.8 K was taken into account by adding a velocity according to the Maxwell distribution. The final velocity is transformed to momentum and this value is then stored in a histogram weighted by the ADK Rate of the electric field at the instant of ionization, assuming that the ADK Rate for circularly polarized light is still a good approximation for the ionization rate of the elliptically polarized pulse with an ellipticity of about 0.9. For each starting time 400 trajectories have been computed, which can be done efficiently by calculating the propagation only once for each starting point and then calculating the initial and thermal velocities independently for each trajectory, since these velocities represent just an offset of the trajectory in velocity space. The intensity is used as a fitting parameter to the experimental data. The best fit was achieved at an intensity of 3.92 10^{14} W/cm^2 resulting in a Keldysh parameter γ gamma of 1.14, which is well within the experimentally estimated values. The use of tunneling based theories for $\gamma > 1$ has been successfully shown by Uiberacker et al. [25]. Our model yields excellent agreement with the experimental data of Eckle et al. [7]. It reproduces the general behavior of shifting the intensity from one lobe of the distribution into the other not only qualitatively but also quantitatively as shown in direct comparison of the measured and calculated angular distributions (Fig. 4).

#129004 - $15.00 USD Received 25 May 2010; revised 23 Jul 2010; accepted 23 Jul 2010; published 2 Aug 2010
(C) 2010 OSA

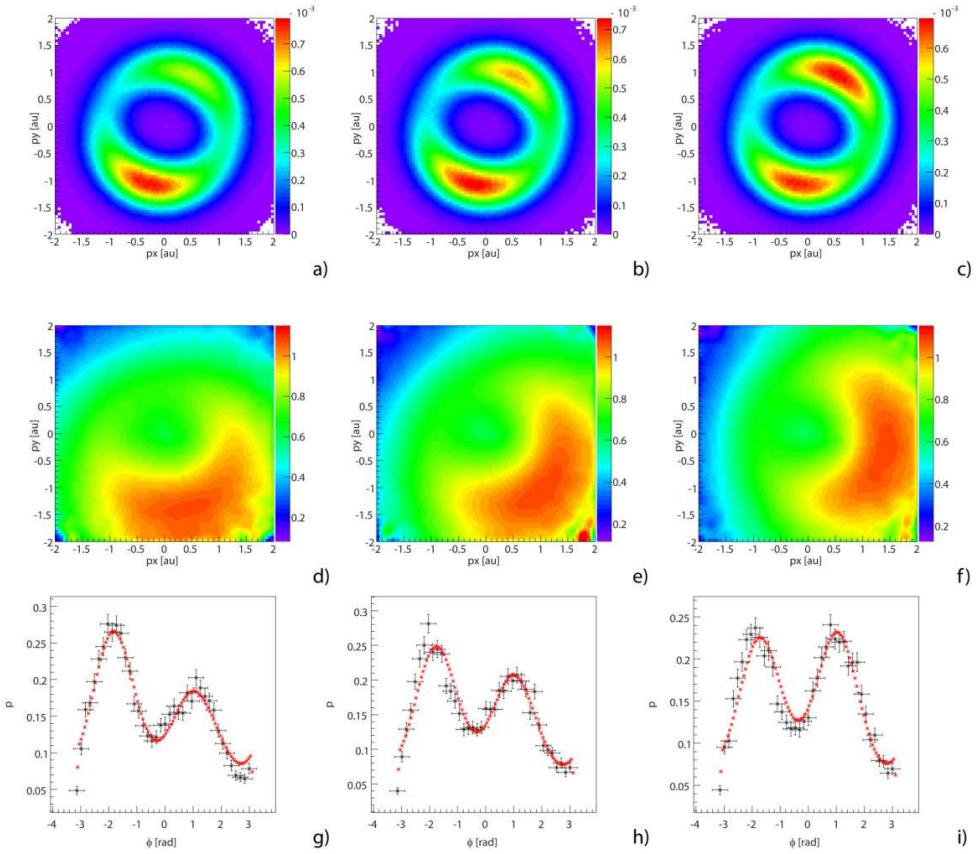

Fig. 4. a) to c): Helium ion momentum distribution, ionized at 3.92 10^{14} W/cm^2. d) to f): as a) to c) but smoothed and normalized with respect to a smoothed distribution with random CEO phase. Panels g) to h): Helium ion angular distribution, comparison theory and experiment: Red - theory, black – experiment [7]. Distributions in each row have the same CEO – phase and the increment between the rows is 0.497 radian.

4. Limitations

For intensities, where depletion of the ground state can be neglected, and the ionization takes place mainly at the peak intensity in the laser field, the laser pulse can be modeled with a Gaussian pulse with the ellipticity in the center of the calculated pulse. This approach is no longer valid, once depletion has to be taken into account [26]. The momentum distribution is strongly influenced by the shape of the laser pulse at the time of ionization, and the ellipticity varies strongly outside the central region of the pulse, as seen in Fig. 3. This effect is illustrated in Fig. 5, showing the different angular momentum distributions calculated using ADK rates for ionization of xenon for circularly polarized light and propagation in a Gaussian pulse at 10^{16} W/cm^2. This picture shows only the general behavior, since in this intensity region, where the peak intensity is far above the over-barrier intensity, the ADK rates are no longer valid. Since the ground state can be depleted almost completely within half a laser cycle, see Fig. 5, more accurate rates are needed for a quantitative calculation. Empirical formulas for the static field ionization rates are known for several elements [27] in the barrier-suppression regime, but the comparison of the ionization probability calculated from these rates and from TDSE calculations shows a significant deviation [27].

#129004 - $15.00 USD Received 25 May 2010; revised 23 Jul 2010; accepted 23 Jul 2010; published 2 Aug 2010
(C) 2010 OSA

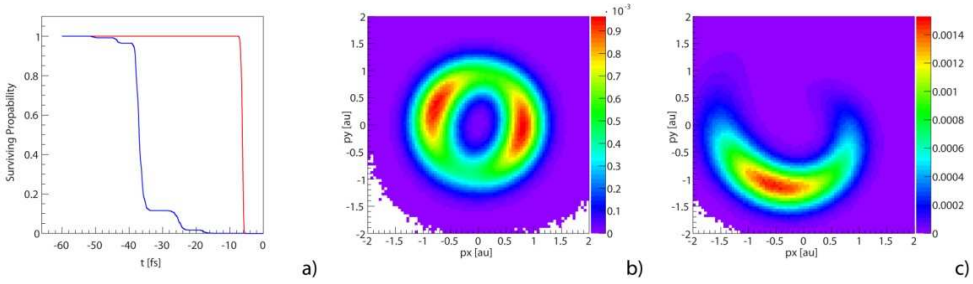

Fig. 5. a): Surviving probability of Xenon for CEO phase stabilized, elliptically polarized laser pulse, FWHM of 5.9 fs and a peak intensity 1 10^{16} W/cm^2. Result for measured pulse (blue) and for a Gaussian pulse matching ellipticity, CEO phase and wavelength of the measured pulse (red). Resulting momentum distribution for the measured pulse b) and for the Gaussian pulse c).

We can neglect the momentum of the ionizing photons, and therefore momentum conservation between the ion and the electron is fulfilled. Thus the forces acting on the particles have the same magnitude and opposite directions. However a limitation of the model is becoming visible when the angular momentum is investigated. For a particle starting in the origin of coordinates with velocity zero the angular momentum L is given by:

$$\vec{L} = \vec{r} \times \vec{p} = \int_{t_i}^{t_f} \int_{t_i}^{t} \frac{q \cdot \vec{E}(\tau)}{m} d\tau dt \times \int_{t_i}^{t_f} q \cdot \vec{E}(\zeta) d\zeta = \frac{q^2}{m} \int_{t_i}^{t_f} \int_{t_i}^{t} \vec{E}(\tau) d\tau dt \times \int_{t_i}^{t_f} \vec{E}(\zeta) d\zeta. \qquad (8)$$

From the q^2 factor in Eq. (8) it follows that the angular momenta of ions and electrons have the same sign and the numerical analysis of this equation shows that L cannot be assumed to be zero. As a consequence the angular momentum has to be provided by the electric field. The time dependence of L and the kinetic energy of the system of ion and electron show two striking features in Fig. 6. The amount of photons needed to provide the kinetic energy is different from the amount of photons needed to provide the angular momentum. The second feature is that the trend is not correct: In the region where the magnitude of the total angular momentum reaches its maximum between its second and third zero crossing, the kinetic energy is continuously increasing. There is a region where the magnitude of the total angular momentum decreases but the total kinetic energy increases. A decrease of angular momentum could be only due to emission of photons while an increase of kinetic energy indicates an absorption of photons. As long emission of low energy photon is excluded, this leads to a contradiction in terms of quantum mechanics. Its origin is the description of the laser field: One could theoretically produce the electric field used in Eq. (3) by a plate capacitor which rotates with frequency ω_0 while the electric field inside the capacitor has the amplitude $A(t)\cdot(\cos^2(\omega_0 t) + \varepsilon\cdot\sin^2(\omega_0 t))^{1/2}$. This external plate capacitor will enforce the angular momentum conservation in a classical picture.

The electric field used in equation Eq. (3) can also be interpreted as the dipole approximation of a laser field, which is usually treated as the solution of the source free Maxwell equation. Classically is not clear how angular momentum conservation can be fulfilled in an electric field having no sources. Newton's third law of motion cannot be fulfilled since there is only one classical particle feeling a force.

One should notice, that by changing the inertial frame to a frame moving with the final velocity of one of the particles and its origin matching the origin of the original frame at the time of ionization the particles initial and final angular momentum vanishes. Since the velocities of the electron and the ion are different, this condition cannot be fulfilled simultaneously for both particles. So even asymptotic angular momentum conservation for $t = \pm\infty$ is not fulfilled.

#129004 - $15.00 USD Received 25 May 2010; revised 23 Jul 2010; accepted 23 Jul 2010; published 2 Aug 2010
(C) 2010 OSA

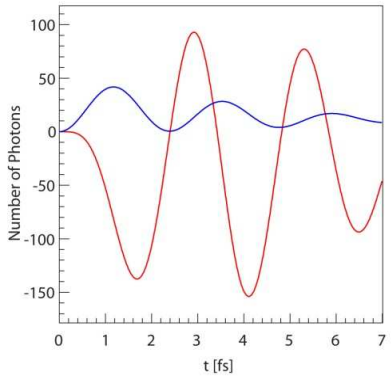

Fig. 6. Total angular momentum in units of ħ (red line) and total kinetic energy (blue line) in units of h·υ for the system of an electron and a Helium ion, ionized at t = 0 with a 5.9-fs Gaussian pulse shape and a peak intensity of 4 10^{14} W/cm^2.

5. Summary

We have analyzed the propagation of an ultra broadband pulse through an achromatic retardation plate and used the calculated field for simulations of the expected momentum distributions. The excellent reproduction of the measured momentum distributions shows the validity of the classical approach to the propagation of the electrons in the laser field and supports the classical mapping of momentum to time. The simplicity and the speed of the computational approach make this method a valuable tool for estimating in advance the quality of the circularly polarized light to be used in experiments and its influence on momentum distributions in ionization experiments as long as depletion plays no role in the reaction, the intensity is below the over-barrier threshold and the angular momentum of single trajectories is not considered.

Acknowledgments

We thank Prof. Reiss, Adrian Pfeiffer, and Dr. Zinner from Bernhard Halle Nachfolger GmbH for fruitful discussions. This work was supported by the Studienstiftung des deutschen Volkes and by the NCCR Quantum Photonics (NCCR QP), research instrument of the Swiss National Science Foundation (SNSF).

#129004 - $15.00 USD Received 25 May 2010; revised 23 Jul 2010; accepted 23 Jul 2010; published 2 Aug 2010
(C) 2010 OSA